Atmos. Chem. Phys. Discuss., https://doi.org/10.5194/acp-2017-1093
Manuscript under review for journal Atmos. Chem. Phys.
Discussion started: 20 December 2017

Atmospheric Chemistry and Physics Discussions

A Comparison of Plume Rise Algorithms to Stack Plume Measurements in the Athabasca Oil Sands

Mark Gordon[1], Paul A. Makar[2], Ralf M. Staebler[3], Junhua Zhang[2], Ayodeji Akingunola[2], Wanmin Gong[2], Shao-Meng Li[3]

1) Earth and Space Science and Engineering, York University
2) Air Quality Modelling and Integration Section, Air Quality Research Division, Atmospheric Science and Technology Directorate, Science and Technology Branch, Environment and Climate Change Canada.
3) Air Quality Processes Research Section, Air Quality Research Division, Atmospheric Science and Technology Directorate, Science and Technology Branch, Environment and Climate Change Canada.

Abstract

Plume rise parameterizations calculate the rise of pollutant plumes due to effluent buoyancy and exit momentum. Some form of these parameterizations are used by most air quality models. In this paper, the performance of the commonly used Briggs plume rise algorithm was extensively evaluated through a comparison of the algorithm's results when driven by meteorological observations with direct observations of plume heights in the Athabasca oil sands region. The observations were carried out as part of the Canada-Alberta Joint Oil Sands Monitoring Plan in August and September of 2013. Wind and temperature data used to drive the algorithm were measured in the region of emissions from various platforms, including two meteorological towers, a radio-acoustic profiler, and a research aircraft. Other meteorological variables used to drive the algorithm include friction velocity, boundary-layer height, and the Obukhov length. Stack emissions and flow parameter information reported by Continuous Emissions Monitoring Systems (CEMS) were used to drive the plume rise algorithm. The calculated plume heights were then compared to interpolated aircraft SO_2 measurements, in order to evaluate the algorithm's prediction for plume rise. We demonstrate that the Briggs algorithm, when driven by ambient observations, significantly underestimated plume rise for these sources, with more than a third of the predicted plume heights falling below half the observed values from this analysis. Including the effects of effluent momentum and choosing between different forms of the parameterizations improve results slightly, but there remains an average underestimation between 4 and 21%, depending on the measurement platform used to drive the algorithm. These results are in contrast to numerous plume rise measurement studies published between 1968 and 1993. It is suggested that further investigation using long-term in-situ measurements with currently available technologies is warranted to investigate this discrepancy.

Atmos. Chem. Phys. Discuss., https://doi.org/10.5194/acp-2017-1093
Manuscript under review for journal Atmos. Chem. Phys.
Discussion started: 20 December 2017

Atmospheric Chemistry and Physics Discussions

1. Introduction

In large scale air-quality models, grid cell sizes may be on the order of 1 km or larger, while vertical resolution may be in the tens to hundreds of meters (c.f. Im *et al.*, 2015). The large scale impacts of transport by winds and turbulence are handled in these models by algorithms dealing with advection and turbulent diffusion of tracers. However, the redistribution of mass from elevated stacks with high-temperature and/or high-velocity emissions sources requires parameterization in order to deal with issues such as the buoyancy and momentum of the emitted mass. Briggs and others developed a system of parameterizations for plume rise beginning in the late 1960's (e.g. Briggs, 1969; Briggs, 1975). The parameterizations followed dimensional analysis to estimate plume rise based on meteorological measurements, atmospheric conditions, and stack parameters. Different variations of the Briggs plume rise parameterization equations are used in three-dimensional air-quality models such as GEM-MACH (Im *et al.*, 2015), CMAQ (Byun and Ching, 1999), CAMx (Emery *et al.*, 2010), as well as AEROPOL, SCREEN3, and CALGRID models (see Holmes, 2006 for a summary of these models). The Briggs equations are also used in the Regional Acid Deposition Model (RADM, Byun and Binowski, 1991), and have been incorporated into emissions processing systems such as SMOKE (CMAS Website) and SMOKE-EU (Bieser *et al.*, 2011a).

As summarized by Briggs (1969), early observation of plume rise incorporated a wide variety of methods. Plumes were visually traced on Plexiglas screens, photographed, compared in height to nearby towers, and measured with lidar. Other techniques included the release of Geiger counters attached to balloons, and the release of balloons from within the stack chimneys. Bringfelt (1968) summarizes other techniques, using either theodolite, cloud height searchlights, or fluorescent particles sampled by aircraft-mounted instruments. Scaled wind tunnel simulations were also used. These observations were used to constrain the plume rise parameterizations and to choose appropriate constants following dimensional analysis (see Bieser *et al.*, 2011b for a summary).

Once a set of equations for plume rise had been developed, further observations were used to test their accuracy. A report of these comparisons (VDI, 1985) summarizes five studies in which plume rise parameterizations were compared to observations. These studies consistently show a tendency to overestimate plume rise using the Briggs parameterizations. Giebel (1979) measured pit coal power plant plumes with lidar which averaged 50% lower than the parameterization. Rittmann (1982) reanalyzed the Bringfelt (1968) and Briggs (1969) measurements from "industrial-sized sources" and found most plume heights were between 12 and 50% of the predicted rise. England *et al.* (1976) measured plume rise at a gas turbine facility with airborne measurements of NO_x and found plumes were 30% lower than predicted. Hamilton (1967) measured power station plumes with lidar which averaged 50% lower than the parameterization. Moore (1974) used data from seven locations measured with a variety of methods (photography, lidar, aircraft, and balloons) and found measured plume rise was 10-20% lower than the parameterization. The authors of the VDI (1985) report recommend reducing the plume height predicted by the Briggs equations by 30% during neutral conditions. No recommended adjustment for stable and unstable conditions was proposed, primarily due to a lack of supporting data. Sharf *et al.* (1993) measured the rise of power plant plumes with

aircraft-based SO_2 measurements and found that plume heights were generally overestimated by the parameterization by up to 400 m. More recently, Webster and Thompson (2002) tested the Briggs equations as well as a more complex Lagrangian model using a network of surface concentration measurements downwind of a power plant. The Briggs algorithm resulted in concentration predictions which were biased high relative to observations, potentially indicating a tendency to underestimate plume rise, as emissions distributed over a lower vertical height would result in higher concentration. Hence, the majority of earlier studies which have been compared to the original Briggs plume rise parameterization indicated some degree of overestimation of the actual plume rise, with a single more recent study suggesting an underestimation of actual plume rise (inferred through surface measurements).

This manuscript evaluates the performance of the Briggs plume rise parameterization, as it is formulated in Environment and Climate Change Canada's GEM-MACH model. For comparison, another model proposed by Briggs (1984) for irregular stability profiles is also evaluated. In the summer of 2013, as part of the Canada-Alberta Joint Oil Sands Monitoring (JOSM) Plan, aircraft measurements and monitoring stations were used to study dispersion and chemical processing of pollutants emitted from sources in the Athabasca oil sands region of northern Alberta. The GEM-MACH model (nested to 2.5 km resolution) was run from August through September, coincident with the measurement campaign, as an aid in directing aircraft flights and in subsequent post-campaign analysis of the observations. The model makes use of the Briggs plume rise algorithms. The large stacks in the region emit many key pollutants, such as SO_2, NO_x, VOCs, CO, and aerosols. The accuracy of the plume calculations thus has significant impact on model predictions, particularly close to the sources. Here, we investigate the plume rise algorithm in a "stand-alone/off-line" sense. In order to remove the potential influence of model wind speed and temperature errors on the algorithm results, we use observations of these and other meteorological variables in the study region to drive Briggs algorithms. We also make use of aircraft observations of emitted SO_2 in order to evaluate the accuracy of the algorithm. For a direct comparison of model output plume location to aircraft observations, along with a study of the impacts of different levels of stack parameter data on model predictions, the reader is referred to the companion paper Akingunola *et al.* (2017, this issue).

Atmos. Chem. Phys. Discuss., https://doi.org/10.5194/acp-2017-1093
Manuscript under review for journal Atmos. Chem. Phys.
Discussion started: 20 December 2017

Atmospheric Chemistry and Physics Discussions

2. Methods

2.1 Plume Rise Parameterization in GEM-MACH.

The plume rise (Δh) calculation in GEM-MACH is driven by 9 variables: stack height (h_s), exit temperature at the stack outlet (T_s), stack emission volumetric flow rate (V), air temperature at stack height (T_a), wind speed at stack height (U), surface temperature ($T_{surface}$), boundary-layer height (H), friction velocity (u_*), and Obukhov length (L). These input parameters are used to generate the rise in the plume above the stack height (Δh), as well as the upper and lower boundaries of the plume having risen to equilibrium. In models such as GEM-MACH, buoyant transport of emissions through that region is assumed to be instantaneous - the emitted mass is distributed through the given region under the assumption that the buoyant plume has reached equilibrium. Here, all of these variables are obtained from observations (either directly or via the use of the appropriate formulae with observed quantities).

The algorithm makes use of derived quantities (the buoyancy flux, F_b, the stability parameter, s, and the convective velocity, H_*) with different formula for plume rise corresponding to *stable*, *neutral*, and *unstable* atmospheric conditions. The buoyancy flux is calculated from Briggs (1984, equivalent to their Eq. 8.35) as

$$F_b = \begin{cases} \frac{g}{\pi} V \frac{(T_s - T_a)}{T_s}, & T_s > T_a \\ 0, & T_s \le T_a \end{cases}, \quad (1)$$

where $g = 9.81$ m s^{-2} is the gravitational acceleration. The stability parameter is calculated from Briggs (1984, combining their Eq. 8.8 and Eq. 8.14) as

$$s = \frac{g}{T_a}\left(\frac{dT_a}{dz} + \frac{g}{c_p}\right). \quad (2)$$

where z is the height coordinate and $c_p = 1005$ J K^{-1} kg^{-1}. The temperature gradient is calculated from the temperature difference over the stack-height ($dT_a/dz = \left(T_a - T_{surface}\right)/h_s$), with a maximum value set at –5 K/km. The convective velocity ($H_* = -2.5u_*^3/L$) is defined in Briggs (1985).

The atmosphere is considered *stable* at the plume height if either $0 < L < 2h_s$ (stable conditions) or $h_s \ge H$ (direct emission above the boundary-layer). From Briggs (1984, their Eq. 8.71), the plume rise is calculated as

$$\Delta h = 2.6\left(\frac{F_b}{sU}\right)^{\frac{1}{3}}. \quad (3)$$

The atmosphere is considered *unstable* if $-0.25h_s < L < 0$. In the unstable case, the plume rise is taken as the minimum value of two formulations of Briggs outlined in Byun and Ching (1999),

$$\Delta h = \min\left[3\left(\frac{F_b}{U}\right)^{\frac{3}{5}} H_*^{-\frac{2}{5}},\ 30\left(\frac{F_b}{U}\right)^{\frac{3}{5}}\right]. \quad (4)$$

Atmos. Chem. Phys. Discuss., https://doi.org/10.5194/acp-2017-1093
Manuscript under review for journal Atmos. Chem. Phys.
Discussion started: 20 December 2017

Atmospheric Chemistry and Physics Discussions

This effectively places a lower limit on the magnitude of the convective velocity in determining plume rise as $H_* > 0.00316$ m^2/s^3 (from $H_*^{-2/5} < 10$). Briggs (1984) gives the example of clear summer conditions as $H_* = 0.007$ m^2/s^3.

The plume is considered *neutral* if $L > 2h_s$ or $L < -0.25h_s$ (or $-4 < \frac{h_s}{L} < 0.5$). The plume rise in neutral conditions is taken as the minimum two formulations of Briggs outlined in Sharf *et al.* (1993) and Byun and Ching (1999) as

$$\Delta h = \min\left[39\frac{F_b^{3/5}}{U}\ ,\ 1.2\left(\frac{F_b}{u_*^2 U}\right)^{3/5}\left(h_s + 1.3\frac{F_b}{u_* U}\right)^{2/5}\right]. \quad (5)$$

The only difference between Eqns. 3, 4, and 5 and the plume rise parameterizations used in SMOKE (described in Bieser *et al.*, 2011 and Houyoux, 1998) is the option of the minimum values in unstable and neutral conditions. In the SMOKE model, only the second parameterizations within the minima of Eqns. 4 and 5 are used. Both the approaches used in GEM-MACH and SMOKE are investigated in the following analysis.

Plume rise is also modified for situations where the stack height is less than the boundary-layer height ($h_s < H$), but the plume rises high enough to penetrate the boundary-layer height to some degree ($h_s + \Delta h > H$). This is referred to as "bumping" (Briggs, 1984). The vertical plume depth is assumed to be equal to the plume rise so that the plume is bound by the height range $h_s + 0.5\Delta h < z < h_s + 1.5\Delta h$. If any portion of the plume is above H, the plume rise is calculated (from Briggs, 1984) as

$$\Delta h = (0.62 + 0.38p)(H - h_s), \quad (6)$$

where p is the fraction of the plume above H (i.e. $p = 0$ if $h_s + 1.5\Delta h = H$ and $p = 1$ if $h_s + 0.5\Delta h = H$).

While the above formulae are used in GEM-MACH and other models, we also examine a layer-based approach suggested by Briggs, described below, and the companion paper (Akingunola *et al.* (2017) examines the impact of this approach within the GEM-MACH model itself.

2.2 Plume Rise into Irregular Stability Profiles (The Layered Method)

In addition to the parameterization discussed above, Briggs (1984) suggests a layer-based approach to calculate plume rise for complex stability profiles. In this approach, the plume buoyancy (F) is modified as it passes through each discrete layer as

$$F = F_j - 0.053 s_j U_j\left(z_c^3 - z_j^3\right) \quad (7)$$

where F_j is the buoyancy flux at the bottom of layer j, s_j is the layer stability, U_j is the wind speed, and z_j is the layer height above ground level (agl). The wind speed in the original Briggs formulation is taken as constant with height, while here we use an average wind speed for each layer. The lower boundary of the first layer is the stack height ($z_{j=0} = h_s$). The value of F is determined sequentially for each layer at the top of each layer (with $z_c = z_{j+1}$) until it becomes

Atmos. Chem. Phys. Discuss., https://doi.org/10.5194/acp-2017-1093
Manuscript under review for journal Atmos. Chem. Phys.
Discussion started: 20 December 2017

Atmospheric Chemistry and Physics Discussions

negative. For the layer where F becomes negative, Eq. 7 is solved to give the plume height z_c for $F = 0$. Plume rise is calculated as $\Delta h = z_c - h_s$. Layer thickness will depend on the vertical model or measurement resolution. For this analysis layer thickness is discussed in Section 2.4.

While the Briggs parameterization discussed in Section 2.1 is driven by surface (or near-surface) observations, the layered method (Eq. 7) is driven by observations up to the height of the plume. The observed plume centreline heights (Section 2.7) vary from between approximately 100 m and 1000 m above the surface. Hence the layered method can be used with the elevated observations from an aircraft measurement platform and an acoustic profiler (Section 2.4). It is noted that this layered method is not currently used in the GEM-MACH model, but we include it here for comparison.

2.3 Stack Height (h_s), Exhaust Temperature (T_s), and Flow Rate (V)

As part of the Continuous Emission Monitoring System (see CEMS, 1998), measurements of 19 stacks in the region of study with valid hourly measurements of SO_2 and average effluent velocity and temperature were obtained from Alberta Environment and Parks. Stacks which emit primarily NO_x and no reported SO_2 are not used in this analysis. The stack locations, elevations, and parameters are summarized in Table 1. A flaring stack at the CNRL facility (which does not require CEMS monitoring) is added to the list (CNRL 4) because daily reports indicated a large amount of SO_2 emissions were released from the flaring stacks for a one-week period during the field study. This flaring stack is parameterized using effluent velocity and temperature based on annual NPRI inventory values (NPRI ID 23275; NPRI Website, see ECCC & AEP, 2016).

For comparison, average effluent velocities and temperatures were calculated for each stack over the 84 hours of research aircraft flight time. The aircraft flight campaign is discussed in more detail in the following section. To calculate the plume rise, the volumetric flow rate was estimated from the diameter and exit velocity as $V = w_s \pi d_s^2/4$. The yearly-averaged SO_2 emission rates for each stack as determined from the Cumulative Environmental Management Association inventory for the year 2010 (see CEMA, 2012) are shown in Table 1. For stacks without reported CEMS SO_2 emission rates, the average CEMA SO_2 emission rate was used to eliminate stacks from the analysis which would not emit enough SO_2 to be observed by the aircraft-based instrumentation, assuming that the emission profiles in 2013 are not significantly different from 2010. Stacks from the Imperial Oil Kearl facility are not in the CEMA inventory because those stacks started operation later than 2010. A comparison of observed plume locations, as outlined below in Section 2.7, demonstrates that the Kearl and Firebag stacks produce no discernable SO_2 plumes.

Based on these values and observations, the stacks Suncor 5-6, CNRL 2-3, Kearl 1-4, and Firebag 1-3 were not used for the plume rise comparison. Hence, the comparison of plume rise is limited to a total of 8 stacks at Suncor (1-4), Syncrude (1,2), and CNRL (1,4). The locations of these 8 stacks are shown in Fig. 1.

The relatively high flow rates and diameters of some stacks may lead to plume rise due to momentum alone, especially under stable conditions. Briggs also developed similar equations

Atmos. Chem. Phys. Discuss., https://doi.org/10.5194/acp-2017-1093
Manuscript under review for journal Atmos. Chem. Phys.
Discussion started: 20 December 2017

for rise due to momentum (c.f. Briggs, 1984). These equations are typically used when $F_b = 0$, and the plume is assumed to be either a vertical jet (momentum driven) or a bent over plume (buoyancy driven). Bieser (2011) gives a momentum plume rise for all stability conditions as

$$\Delta h_m = 3.0\left(\frac{d_s w_s}{U}\right). \quad (8)$$

For a wind speed of $U = 1$ m s^{-1}, the resulting momentum rise ranges from 2 m to 285 m for the stack parameters listed in Table 1. Hence momentum rise may be significant and a more detailed parameterization is employed in Section 4.4.2 for comparison.

Table 1. CEMS stack parameters for all stacks within flight area, including location and elevation at the stack base ($z_{surface}$), stack height (h_s), stack diameter (d_s), effluent velocity at the stack exit (w_s), and effluent temperature at the stack exit (T_s). SO_2 values are average yearly emission rates from the CEMA 2010 stack inventory. All stacks for the Imperial Oil Kearl mining facility are not available in the CEMA 2010 inventory because the Kearl facility began production in spring 2013. Stack numbers (#) are for identification within this analysis and do not represent official reporting ID.

Facility	#	Latitude	Longitude	$z_{surface}$ [m amsl]	h_s [m]	d_s [m]	w_s[m/s]	T_s [K]	SO_2 [g/s]
Suncor*	1	57.0020	-111.4770	257	106.7	5.8	<0.1	404.3	140.3
Suncor*	2	57.0050	-111.4770	254	106.7	2.0	9.3	711.5	55.5
Suncor*	3	57.0030	-111.4770	256	137.2	7.0	<0.1	336.3	189.0
Suncor*	4	57.0060	-111.4790	255	106.1	3.4	4.2	947.3	165.9
Suncor	5	57.0090	-111.4790	247	60.7	3.4	4.8	484.5	0.8
Suncor	6	57.0100	-111.4860	260	42.7	3.5	4.1	428.8	1.1
Syncrude*	1	57.0410	-111.6160	304	183.0	7.9	12.0	472.9	2269.1
Syncrude*	2	57.0480	-111.6130	305	76.2	6.6	10.1	350.7	122.2
CNRL*	1	57.3390	-111.7380	284	106.7	3.4	4.1	851.1	197.3
CNRL	2	57.3370	-111.7400	286	61.0	3.9	9.2	453.9	0.5
CNRL	3	57.3360	-111.7320	283	38.0	5.5	8.6	464.9	0.2
CNRL*	4	57.3390	-111.7380	284	109.0	1.4	6.2	1273.1	N/A+
Kearl	1	57.4002	-111.0703	360	30.0	3.0	5.9	409.6	N/A
Kearl	2	57.4002	-111.0709	358	30.0	3.0	6.0	421.4	N/A
Kearl	3	57.4002	-111.0712	357	30.0	3.0	6.1	419.9	N/A
Kearl	4	57.4002	-111.0706	359	30.0	3.0	5.9	433.9	N/A
Firebag	1	57.2309	-110.8458	593	55.0	0.7	4.4	833.2	4.4
Firebag	2	57.2359	-110.8530	600	27.0	5.5	9.4	456.0	2.2
Firebag	3	57.2359	-110.8478	596	30.0	1.7	10.9	480.9	4.6

* Based on SO_2 emissions and flight observations, only these 8 stacks are used for the plume rise analysis.
+ The CNRL#4 flaring stack is added based on NPRI inventory and is assumed to emit significant SO_2 for a 1-week period during the field study.

2.4 Measurement Platforms

Wind speed (U), wind direction (θ), and temperature (T_a) data at the stack height and at the surface were estimated based on measurements made at either: one of two meteorological towers in the study region (WBEA: AMS03 and AMS05); or a radio-acoustic sounding system

Atmos. Chem. Phys. Discuss., https://doi.org/10.5194/acp-2017-1093
Manuscript under review for journal Atmos. Chem. Phys.
Discussion started: 20 December 2017

Atmospheric Chemistry and Physics Discussions

(*wind*RASS, Scintec). Figure 1 demonstrates the sites of the WBEA meteorological towers, and the radio-acoustic sounding system (RASS).

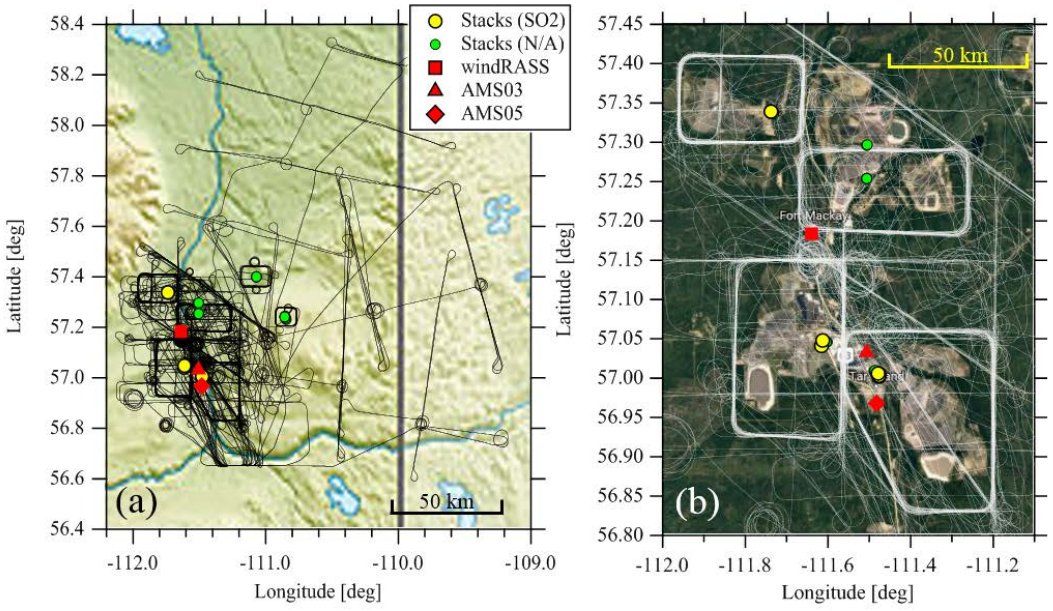

Figure 1. The flight tracks (black lines on (a), white lines on (b)) during the 22 flights of the JOSM study, compared to the location of the facility stacks, including SO_2 emitting stacks (yellow circles) and non-SO_2 emitting stacks (green circles), the radio-acoustic profiler (windRASS, red square), the WBEA meteorological towers: AMS03 (red triangle); and AMS05 (red diamond). Stack towers in close proximity are overlapping. The relief map (a) shows the extent of the flight area and the Athabasca river valley with the Alberta/Saskatchewan border shown at –110° longitude (Wikipedia, credit: Carport). The satellite image (b) is a close up in the region of the facilities (Google: Landsat/Copernicus, 2017).

The AMS03 tower measures wind speed, wind direction and temperature at heights of 20, 45, 100, and 167 m (all heights above ground level). The AMS05 tower measures wind speed and direction at heights of 20, 45, 75, and 90 m and temperature at heights of 2, 20, 45, and 75 m. Tower measurements are reported as 1-hour averages. The RASS measures wind speed and temperature (among other variables) between a minimum height of 40 m and a maximum height which varies depending on wind conditions (Cuxart *et al.*, 2012). During the aircraft flight period, the maximum RASS measurement height varied from 130 m to 800 m, with an average 336 m. The RASS measurements are 15-min averages.

As part of JOSM, aircraft-based measurements were made in the Athabasca oil sands region between August 13 and September 7, 2013. The project included 22 flights, which were flown in some combination of either box formations (circumnavigating a facility at variable heights in order to determine facility pollutant emissions), screen formations (flown perpendicular to the plume centreline axis to characterize the transformation of the plumes), spiral ascent and descent (to characterize boundary-layer structure), or horizontal area coverage (to verify satellite

Atmos. Chem. Phys. Discuss., https://doi.org/10.5194/acp-2017-1093
Manuscript under review for journal Atmos. Chem. Phys.
Discussion started: 20 December 2017

Atmospheric Chemistry and Physics Discussions

observations over a larger spatial extent). Figure 1 shows all these flight formations. Within the 22 flights, there were 16 box-flight formations and 21 screens used for this analysis. Aircraft flight times varied from approximately 2.5 hours to over 5 hours, typically in the mid-afternoon, for a total of 84 hours. Wind speeds and temperatures were measured from the aircraft with a Rosemount 858 probe, sampled at 32 Hz and averaged to 1 Hz. For details of the aircraft measurements, see Li *et al.* (2017), Liggio *et al*. (2016), and Gordon *et al*. (2015). The aircraft flew at a minimum height of 150 m above ground level (agl). The maximum height of box formations varied from 500 m agl to 1300 m agl, while the maximum height of screen formations ranged from 350 m agl to 2000 m agl.

Table 2. Correlation coefficient (R^2) of wind speeds (U), wind directions (Ψ), and temperature (T) at a height of 90 m (AMS03), 100 m (AMS05 and RASS), or < 200 m (aircraft).

		R^2		
		U	Ψ	T
RASS	AMS03	0.61	0.88	0.84
AMS03	AMS05	0.80	0.94	0.98
AMS05	RASS	0.56	0.84	0.82
Aircraft	RASS	0.66	0.60	0.82
Aircraft	AMS03	0.61	0.63	0.78

Tower, RASS, and aircraft measurements were compared over the 84 flight hours. The RASS was not operational until Aug. 17 (thus missing 3 flights); hence RASS data are compared for a reduced period. For comparison to the tower measurements, the 15-min RASS and 1-s aircraft measurements were averaged to concurrent 1-hour values. For comparison to the RASS, the 1-s aircraft measurements were averaged to 15-min values. The resulting correlation coefficients are listed in Table 2. The aircraft winds and temperature measurements are also compared with the highest tower (AMS03) and the RASS. RASS measurements were compared at a height of 100 m. In the case of AMS03, the measurement at a height of 167 m was compared to all concurrent aircraft measurements below 200 m. The wind speed comparisons are best between the two towers ($R^2 = 0.80$). Wind direction compares well for the towers and the RASS ($R^2 > 0.84$). Temperature compares well for all measurement platforms ($R^2 > 0.78$). Generally, comparisons with the aircraft give the lowest correlation values.

We note that the Athabasca oil sands region is centered on the Athabasca River valley, with over 500m of vertical relief within 60 km of the facilities; the flow within the valley may be complex, with frequent observations of shear between plumes from stacks at different elevations under stable conditions. The low correlations between the stations and between the stations and the aircraft reflect this variation in local meteorological conditions.

Atmos. Chem. Phys. Discuss., https://doi.org/10.5194/acp-2017-1093
Manuscript under review for journal Atmos. Chem. Phys.
Discussion started: 20 December 2017

Atmospheric Chemistry and Physics Discussions

2.5 Stability (z/L), Boundary-Layer Height (H), and Friction Velocity (u_*)

Stability, boundary-layer height, and friction velocity were all determined from the observations using wind speed and temperature profiles from multiple height measurements. The towers, which have anemometers and temperature sensors at variable heights between 2 m and 167 m, measured within the surface layer and are best suited for these estimations. The RASS, which has a minimum measurement height of 40 m, may not capture the surface layer effectively. As the aircraft did not fly below a height of 150 m, aircraft-based measurements cannot be used to estimate the stability, boundary-layer height, and friction velocity. For our analysis, we calculate L, H, and u_* to drive the Briggs parameterization (Eqns. 1-6) using observations from the two towers (AMS03 and AMS05) and the RASS.

The atmospheric stability is determined using the Bulk Richardson Number, which is defined (Garratt, 1994) as

$$R_i = \frac{g z_h}{T} \frac{\Delta T}{\Delta U^2}. \tag{9}$$

Here ΔT and ΔU are the temperature and wind speed differences over the height range (z_h). The height range is determined as the difference in height between the highest measurement location and the lower measurement location. For example, z_h =147 m for AMS03, z_h = 55 m for AMS05, and z_h is variable for the RASS. The Richardson number is then related to the stability parameter (Kaimal and Finnigan, 1994) as

$$\frac{z}{L} = \begin{cases} R_i & \text{for } R_i < 0 \\ \dfrac{R_i}{1 - R_i/R_{ic}} & \text{for } 0 < R_i < R_{ic} \\ +\infty & \text{for } R_i > R_{ic} \end{cases} \tag{10}$$

Here $R_{ic} = 0.25$ is the critical Richardson number, chosen as the mid-range of reported values (0.2, 0.25, or 0.5; Mahrt, 1981). For $R_i > R_{ic}$ there is no solution, so this is modelled as extremely stable boundary-layer with L slightly larger than zero (to satisfy the stability condition $L > 0$).

Boundary-layer height can be parameterized for stable and unstable conditions following Mahrt (1981) as

$$H = \frac{R_i T_{sur}}{g} \frac{U(H)^2}{T(H) - T_{surface}}, \tag{11}$$

where R_i is the bulk Richardson number and $U(H)$ and $T(H)$ are the respective wind speed and temperature at the boundary-layer height. Since measurements at the boundary layer height may not be available, we approximate the wind speed to temperature gradient ratio in Eq. 11 as $U(z_{max})^2/\big(T(z_{max}) - T_{surface}\big)$, where z_{max} is the highest measurement height of 167 m, 90 m, or up to 800 m for AMS03, AMS05, and the RASS respectively.

The boundary-layer height derived from Eq. 11 can be compared to the boundary-layer height estimated from in-situ aircraft measurements of the CH_4 mixing ratio during vertical profile flight formations. These CH_4 profiles demonstrate a well-defined background level above a given height, with elevated CH_4 mixing ratios below this height. The boundary-layer heights

Atmos. Chem. Phys. Discuss., https://doi.org/10.5194/acp-2017-1093
Manuscript under review for journal Atmos. Chem. Phys.
Discussion started: 20 December 2017

Atmospheric Chemistry and Physics Discussions

determined by the aircraft measurements range from 340 m to 1790 m with an average of 1180 m. The values of H derived from Eq. 11 using the AMS03 tower data for the same time periods as the flights range from 460 m to 3050 m, with an average of 1160 m.

The friction velocity (u_*) was determined from the wind speed profile (Garratt, 1994) as

$$u(z) = \frac{u_*}{k}\left[\ln\left(\frac{z}{z_o}\right) - \Phi\right], \tag{12}$$

where z_o is the roughness length, $k = 0.4$, and the stability parameter is

$$\Phi = \begin{cases} 2\ln\left(\frac{1}{2}(1+x_o)\right) + \ln\left(\frac{1}{2}(1+x_o^2)\right) - 2\,\mathrm{atan}(x_o) + \frac{\pi}{2}, & \text{for } \frac{z}{L} < 0 \\ -5\frac{z}{L} & \text{for } \frac{z}{L} > 0 \end{cases} \tag{13}$$

with $x_o = (1 - 16z/L)^{1/4}$. A least-squares method is used for each hourly profile to determine an appropriate z_o for the measurement location, which is taken as the median value of all the hourly fits. This median z_o value calculated using this method varies considerably by location (1.5m for AMS03, 0.75 m for AMS05, 10.1 m for RASS). The median z_o values were then used to calculate u_* using the hourly wind speed measured at the highest location. The calculation of u_* with the RASS may be inaccurate due to the lack of measurements between the surface and a height of 40 m. However, the large difference in values of z_o may be also due to the different environment surrounding the measurement locations, since the towers are surrounded by forest and the RASS is located in the town of Fort McKay.

2.6 Stability Profile Measurements for the Layered Method

To drive the layered method discussed in Section 2.2, profiles of temperature and wind speed were derived for each box and each screen using RASS and aircraft observations. RASS layers were 10 m thick to match the instruments resolution. The lowest RASS measurement is at a height of 40 m, well below the lowest stack height (76 m). Because the maximum observation height of the RASS varies (with an average of 336 m), it was necessary to extrapolate temperature and wind speed above the maximum measurement height in some cases. This was done by assuming a constant wind speed and a constant temperature lapse rate, based on measurements in the highest 100 m of observations.

For aircraft observations, the box and screen flights were designed to approximate 100 m vertical spacing between each box circuit or screen pass. Based on this resolution we use a layer thickness of 100 m for the layered method driven by aircraft observations. Testing demonstrates that the algorithm is not sensitive to the layer thickness. Flight measurements of wind (U) and temperature (T) for each box and screen are averaged in vertical layers within the 100 m spacing. Since there are no measurements below a height of 150 m agl, the temperature at the lowest layer ($0 < z < 100$ m) is extrapolated by assuming a constant lapse rate and stability below 200 m (i.e. $s_{j=1} = s_{j=0}$). There are no cases of calculated plume height based on the layered method exceeding the maximum aircraft measurement height and hence no need for upward extrapolation of the measurements.

Atmos. Chem. Phys. Discuss., https://doi.org/10.5194/acp-2017-1093
Manuscript under review for journal Atmos. Chem. Phys.
Discussion started: 20 December 2017

Atmospheric Chemistry and Physics Discussions

2.7 Measured Plume Heights and Stack to Plume Matching Algorithm

The aircraft measured numerous pollutants, of which SO_2 is used here to define the stack plume locations since approximately 95% of the SO_2 emissions in the region originate in stacks (Zhang *et al*., this issue). The SO_2 analyzer (Thermo Fisher Scientific, model 43i) on the aircraft measured at a rate of 1 Hz. The flight paths were designed to create a 100 m spacing between measurement points (in both horizontal, *s*, and vertical, *z*) in order to optimize interpolation of the measurements. The measurements were interpolated in *s* and *z* using simple kriging as outlined in the Topdown Emission Rate Retrieval Algorithm (TERRA; Gordon *et al*., 2015). This creates two-dimensional images of SO_2 mixing ratio. For box flights, which circumnavigate the facilities, the *s* coordinate is the distance along the box in the counter-clockwise direction from the southeast corner. For screens, *s* is the lateral distance along the screen, generally perpendicular to the wind direction. Below the lowest flight path (at 150 m agl), no interpolation is performed and the screen is left blank between this level and the ground. Figures 2 and 3 show example box and screen flight paths in both horizontal (Fig. 2) and vertical (Fig. 3) profiles.

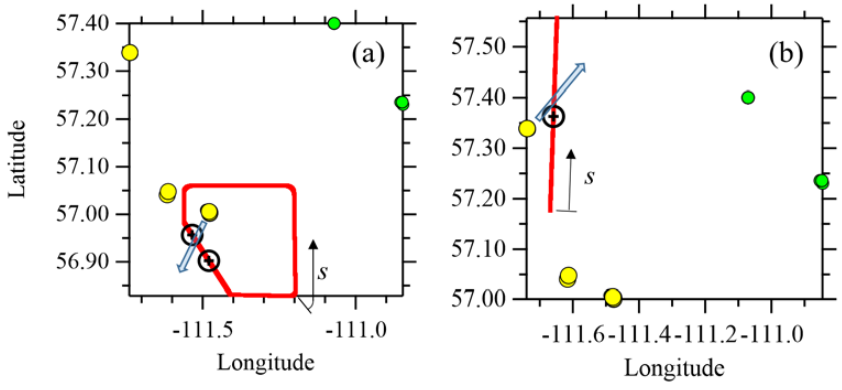

Figure 2. Example horizontal flight path of a box flight (a) and a screen flight (b). Flight paths for the box and screen portion of the flight shown as red lines. Stack locations are shown as filled yellow circles (SO_2 emitting) and green circles (non-SO_2 emitting). The blue arrow shows the forward trajectory of the plume using the average wind direction during each flight segment. The plume locations determined by observations (Fig. 3) are shown as black cross-hairs on the flight paths. The location of the flight path coordinate *s* origin is labeled in each figure.

A semi-empirical approach was used to match each stack to the observed plume locations. The wind direction measured from the aircraft was averaged for the duration of each box or screen. Tower or RASS-based wind direction measurements were not used, as an initial comparison of wind directions and observed plume locations demonstrated that the aircraft measurements are a better representation of the wind direction associated with plume transport than surface

Atmos. Chem. Phys. Discuss., https://doi.org/10.5194/acp-2017-1093
Manuscript under review for journal Atmos. Chem. Phys.
Discussion started: 20 December 2017

Atmospheric Chemistry and Physics Discussions

measurements. This agreement is most likely due to the consistent proximity of the aircraft to the stack sources; the towers and RASS locations can often be much further away (Fig. 1).

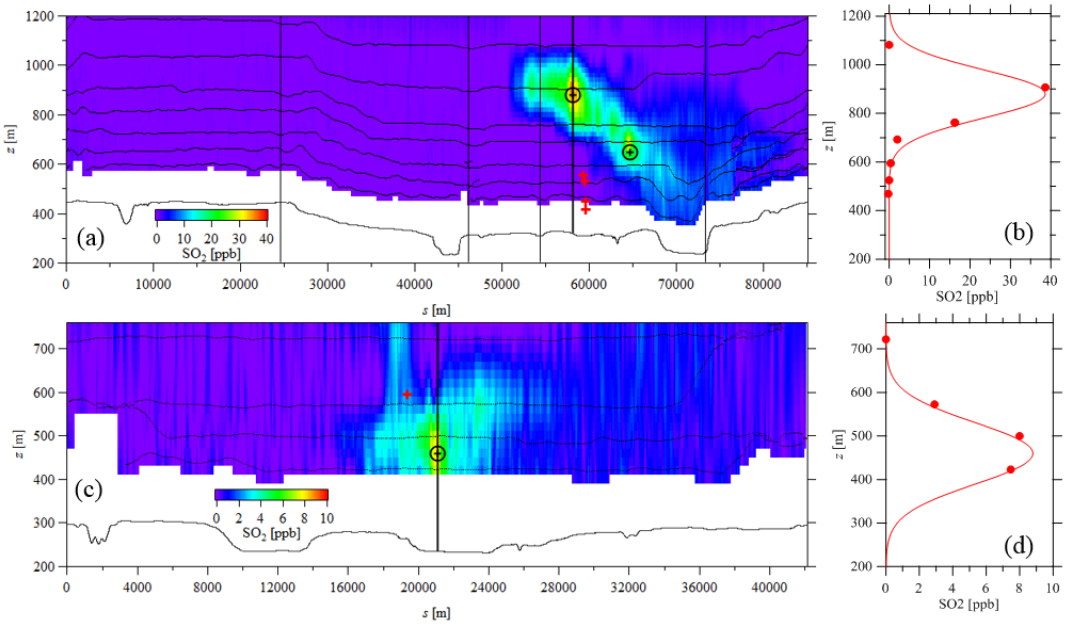

Figure 3. The interpolated images for the box flight (a) and the screen flight (c) (as Fig. 2). The aircraft flight paths are marked by the finely spaced (1 Hz) black dots. The surface location ($z_{surface}$) is shown below the flight path. Interpolation is removed between the lowest flight path and the surface, following the TERRA method. In the box (a), the thin vertical lines show the box corners (see Fig. 2a). The plume locations determined by the Briggs plume rise and the forward trajectories (s_{int}, z_h) are marked by red plus signs. The plume locations determined by observations (s_p, z_p) are shown as black cross-hairs. The Gaussian fitting used to improve plume height estimation is demonstrated (b,d) for the location marked by the thick vertical black line in each image.

The average wind directions were then used to predict the direction of plume transport downwind of each stack. The intercept of each plume's predicted path with the box or screen (s_{int}) was calculated based on this forward trajectory from the stack source to the box or screen intercept. Example box and screen flight paths, forward trajectories, and observed plume locations are shown in Figure 2 for the flights on Aug. 29 (Fig. 2a) and Aug. 15 (Fig. 2b). This simple forward trajectory methodology ignores the local effects of topography, vertical winds, and the variability of the wind during the box or screen segment of each flight (typically less than 2 hours of flight time). Some screens were flown up to 150 km from the 8 stacks (see Fig. 1). Since other stratification, topography, and diffusion effects may influence a plume height at such a large distance from the plume origin, we restrict our analysis to box walls and screens within 50 km of the plume stack sources.

Plume rise (Δh) was calculated for each stack based on the Briggs parameterization, the observed meteorological conditions at the tower or RASS locations, and the CEMS stack parameters, all averaged for the duration of the box or screen flight periods. This calculation also defined the estimated plume centreline location at each box or screen as (s_{int}, z_h), where $z_h = z_{surface} + h_s + \Delta h$ and $z_{surface}$ is the surface elevation (amsl) at the intercept.

The flight path observations are converted to two-dimensional (s, z) images by kriging interpolation following the method outlined in Gordon *et al.* (2015). Example interpolated images from both a box and a screen flight are shown in Figure 3. A disadvantage of kriging interpolation of the aircraft data is that the maxima of the plumes will always be fixed at a flight measurement location. To improve the resolution of observed plume height from the interpolated images, the aircraft measurements within a 100-m wide window (i.e. s ± 50m) are fitted to a Gaussian vertical profile. Example profiles are shown in Figures 3b and 3d, which correspond to the windows shown as thick black lines through the maximum SO_2 locations (the plume centres) in Figures 3a and 3c. The maxima of the Gaussian fits for each identified plume are then used to identify the prominent plume locations as (s_p, z_p). The identified plume locations are visually compared to the predicted Briggs plume locations based on the forward trajectories for each box or screen (s_{int}, z_h).

Each calculated plume location (s_{int}, z_h) was paired with each nearby observed plume location (s_p, z_p) to maximize the correlation of calculated and observed plume heights. For example, the calculated plume rise from three stacks would be paired with three observed plume heights by matching the lowest calculated plume height to the lower observed plume height; the middle calculated plume height to the middle observed plume height; and the highest calculated plume height to the highest observed plume height. This gave the highest correlation between predicted values and observations. For a single plume observation and multiple SO_2-emitting upwind stacks, the stack plumes were assumed to have merged and the calculated plume height for each stack was paired to the same observed plume height.

For the example of the Aug. 15 screen flight (Fig. 2b and Figs. 3c,d), the forward trajectory and Briggs algorithm model intercept the flight screen approximately 2 km further south, and 140 m higher, than the observed plume centre, indicating the possibility of more complex wind flow than a simple trajectory. In the example of the Aug. 29 box flight (Fig. 2a and Fig. 3a,b), there are two observed plumes along the NW-SE oriented wall of the box. The forward trajectory model places the plume intercept between these two plumes, closer to the vertically higher and more northern observed plume at the horizontal location given by s = 58 km. There are four stacks within the box, two of which have calculated intercept heights near z_h = 540 m and two of which have calculated intercept heights near z_h = 430 m. All four calculated values are clearly well below the observed intercept heights (z_p = 650 m and 880 m). This demonstrates some ambiguity and subjectivity in this analysis, as four calculated plume locations must be matched to two observed plumes. As described above and for the purposes of statistical comparisons, we match the highest two modeled plumes (near heights of 540 m) with the highest observed plume (880 m) and the lower two modeled plumes (near heights of 430 m) with the lower observed plume (650 m).

Atmos. Chem. Phys. Discuss., https://doi.org/10.5194/acp-2017-1093
Manuscript under review for journal Atmos. Chem. Phys.
Discussion started: 20 December 2017

Atmospheric Chemistry and Physics Discussions

3. Results

3.1 Comparison of Measurement Platforms

The topography of the Athabasca oil sands region can be generally described as a north-south river valley approximately 1 to 5 km in width, within a larger and more gradually sloped north-south valley between 10 and 50 km in width, and up to 500 m of vertical relief (Fig. 1a). Local surface wind patterns can be heterogeneous, especially within the valley. The AMS03 and AMS05 towers are in the vicinity of the Suncor stacks and the Syncrude stacks (Table 1), while the RASS is nearly equidistant to the 8 stacks used for this analysis (Fig. 1b).

As an approximate measure of the uncertainty associated with local meteorology, plume rise values from the 8 stacks are compared using the Briggs parameterization (Eqs. 1-6) with all 3 meteorological measurement platforms (i.e. AMS03, AMS05, and RASS) as well using the layered method (Eq. 7) with both RASS and aircraft measurements. This comparison was done for all concurrent times during which the aircraft was flying box or screen patterns. There were approximately 26 hours during which the aircraft flew in a box pattern and 20 hours during which the aircraft flew in a screen formation, for a total of more than 46 hours. The resulting distributions of calculated plume heights for these 46 hours of flight time for the 8 stacks are compared in Figure 4.

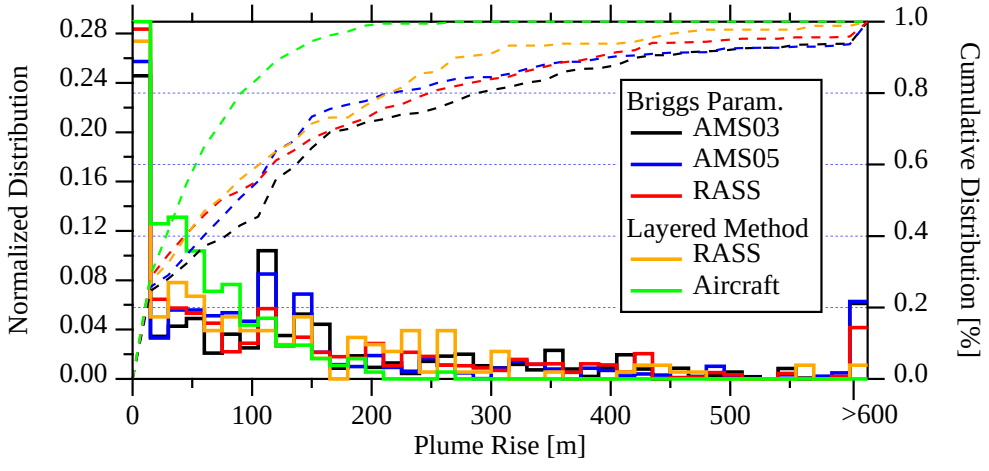

Figure 4. The distribution of calculated plume rise (Δh) using Briggs parameterization (Eqns. 1-6) with input data from the AMS03 and AMS05 towers and the RASS profiler, and using the layered method (Eq. 7) with input date from the RASS profiler and the aircraft. Distributions are shown for each hour (using the 46 hours of box and screen flight times) and for all of 8 SO_2 emitting stacks combined. The right-most histogram bin is the sum of all values of $\Delta h > 600$ m. Cumulative distributions shown by dashed lines.

The distributions of plume rise heights are similar for the Briggs parameterization with the three fixed, near-surface measurement platforms. Approximately 90% of the plume rise values calculated with the AMS tower and RASS measurements are below approximately 400 m, with half or more below 100 m. With the layered method, the plume heights calculated with the RASS measurements are similar to those calculated with the Briggs parameterization. The plume rise heights calculated with the layered method based on aircraft measurements are much lower. Nearly all (99%) of these plumes reach neutral buoyancy at less than 200 m above stack height and more than 80% have plume rise values below 100 m. The average Δh value for both methods and all measurement platforms ranges from 54 m (aircraft) to 161 m (AMS03) and the median Δh value ranges from 40 m (aircraft) to 112 m (AMS03).

3.2 Predicted Plume Rise

The plume rise was calculated for each flight for each stack with the Briggs parameterization for each input (towers, RASS) as well as with the layered method (RASS, aircraft). These plume rises were then paired with the measured plume locations following the method described in Section 2.7. For simplicity, the parameterized plume rise is described as $h_B = \Delta h$, and the observed plume rise is described as $h_M = z_p - z_{surface} - h_s$. Results of this comparison are shown in Figure 5. The analysis resulted in 87 stack to observed plume pairings, for each measurement platform. (Note that a smaller number of pairings were possible for the RASS, which was not in operation for 4 of the 22 flight days). Table 3 compares the results for each measurement method. The low slopes (b <0.5) and significant intercepts ($88 < a <$ 180 m), and low correlation coefficients ($r^2 \leq 0.2$) demonstrate that the Briggs parameterization of plume rise was a poor predictor of actual plume rise. Although the slopes are low, there is more than a 99% confidence (calculated from the standard error of the slopes) that the slopes are significantly different from zero for all cases.

Using the tower or RASS measurements with the standard Briggs parameterization suggests an average underestimation (based on the average ratio) between 26% (AMS03) and 30% (AMS03). The layered method using the RASS and aircraft-based measurements predicts a plume rise that is, on average, 57% or 51% of the observed value, respectively. In all cases, between one-third and half of the plume rise values are underestimated by more than a factor of 2, and between 47 to 60% of predicted plume rise values are within a factor of 2 of the observations.

Use of the RASS observations with both the standard Briggs parameterization of Eqns. 1-6 and the layered method of Eq. 7 allows for a direct comparison between these two approaches. Although the layered method results in more predicted plume rise values within a factor of 2 of the observations (60% compared to 52%), the average ratio (predicted to measured) is lower using the layered method (0.57 compared to 0.70 for the Briggs parameterization). Hence neither method appears to be significantly better for predicting plume rise.

Atmos. Chem. Phys. Discuss., https://doi.org/10.5194/acp-2017-1093
Manuscript under review for journal Atmos. Chem. Phys.
Discussion started: 20 December 2017

Atmospheric Chemistry and Physics Discussions

Table 3. Statistics comparing the predicted to measured plume rises using both the Briggs parameterization (Eqns. 1-6) and the layered method (Eq. 7). The intercept (a) and slope (b) of least-squares fit, average ratio of all values ($\sum h_{B,i}/\sum h_{M,i}$), correlation coefficient (r^2), and fraction of individual ratios of $h_{B,i}$: $h_{M,i}$ below the 1:2 ratio (<0.5), within a factor of 2 (>0.5 & <2), and above the 2:1 ratio (>2). Statistics are recalculated for the tower and RASS with the removal of the minimum option used in Eqns. 4 and 5 (Section 4.4.1) and including plume rise due to stack initial effluent momentum in addition to the removal of the minimum option (Section 4.4.2).

	a [m]	b	Ratio	r^2	Ratio < 0.5	>0.5 & <2	Ratio > 2
Briggs Parameterization, Buoyancy Rise Only							
AMS03	88	0.51	0.74	0.17	39%	57%	3%
AMS05	96	0.44	0.69	0.14	41%	55%	3%
RASS	179	0.24	0.70	0.07	43%	52%	5%
Layered Method							
RASS	131	0.22	0.57	0.17	40%	60%	0%
Aircraft	159	0.09	0.51	0.05	52%	47%	1%
Briggs Parameterization with Removal of Minimum Functions							
AMS03	88	0.64	0.87	0.15	37%	55%	8%
AMS05	101	0.46	0.73	0.14	41%	54%	5%
RASS	211	0.18	0.73	0.03	40%	55%	5%
Briggs Parameterization with Momentum and No Minimum Combined							
AMS03	80	0.75	0.96	0.14	37%	52%	11%
AMS05	103	0.52	0.79	0.12	40%	52%	8%
RASS	208	0.26	0.80	0.05	34%	60%	6%

Atmos. Chem. Phys. Discuss., https://doi.org/10.5194/acp-2017-1093
Manuscript under review for journal Atmos. Chem. Phys.
Discussion started: 20 December 2017

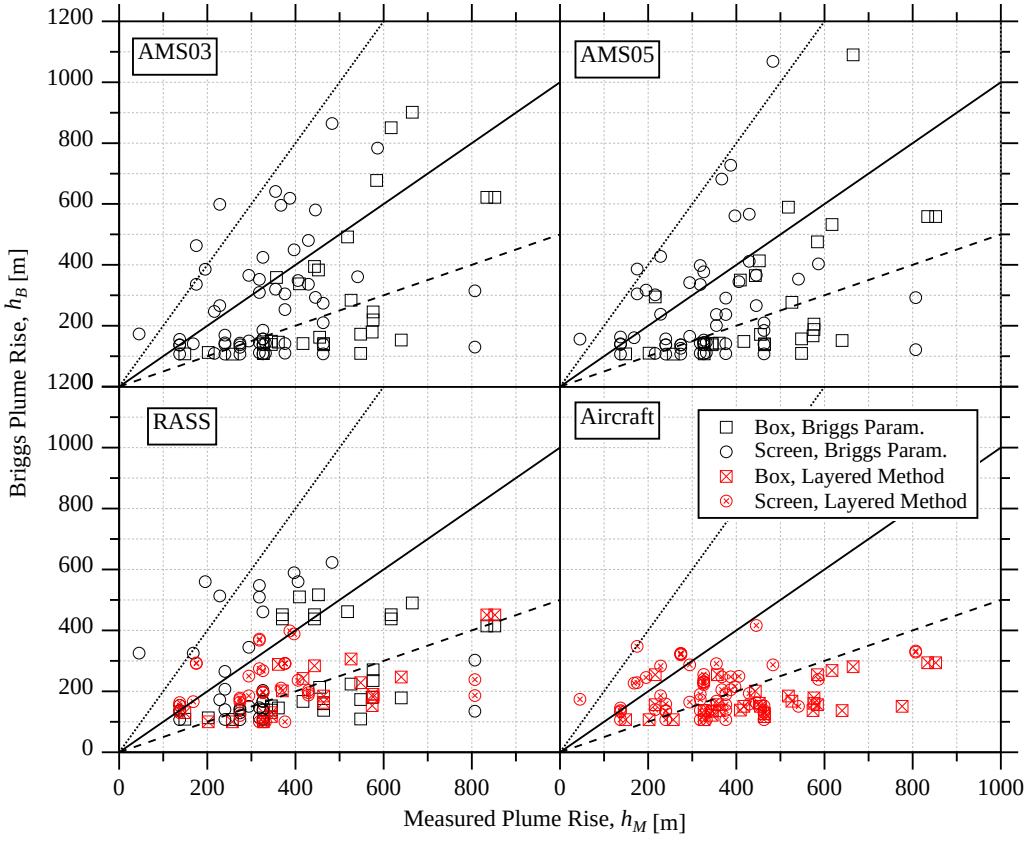

Figure 5. Comparison of the predicted plume rise from the Briggs parameterization used in GEM-MACH with the measured plume rise as determined by various atmospheric measurements as described in the text. Box flights are shown as squares and screen flights are shown as circles. Black markers indicate the Briggs parameterization (Eqns. 1-6) and red indicate the layered method (Eq. 7). Lines demonstrate 2:1 (dotted), 1:1 (solid), and 1:2 (dashed) ratios for comparison.

Atmos. Chem. Phys. Discuss., https://doi.org/10.5194/acp-2017-1093
Manuscript under review for journal Atmos. Chem. Phys.
Discussion started: 20 December 2017

Atmospheric Chemistry and Physics Discussions

4. Discussion

4.1 Stability Classification

Table 4 lists the frequency of each stability class during box and screen flight times according to each measurement platform as determined by the sign and magnitude of the Obukhov length (L). Stable classification is separated as either due to small positive values of $0 < L < 2h_h$, or stack height above the boundary layer height ($h_s > H$). The RASS and the two towers give similar, predominantly (75 to 92%) neutral, stability during the flights, with AMS05 indicating the highest frequency (92%) of neutral conditions. Of these three measurement platforms, only the measurements of the RASS predicts plume rise through stable conditions, due a parameterized boundary layer height that is lower than the stack height.

Table 4. Frequency of each stability type during flight times determined by each measurement platform. Stability is either determined by parameterization of Obukhov length (L, see Section 2.1) or by comparison of the temperature profile with the dry adiabatic lapse rate (Γ).

	Basis	Unstable	Neutral	Stable ($h_s < H$)	Stable ($h_s > H$)
AMS03	L	13%	87%	0%	0%
AMS05	L	8%	92%	0%	0%
RASS	L	6%	75%	0%	19%
RASS (<100m)	Γ	4%	7%	89%	
RASS (>100m)	Γ	13%	33%	53%	
Aircraft (>150m)	Γ	8%	23%	69%	

Stability was determined using the RASS and aircraft temperature profile measurements based on a comparison of the temperature profile to the adiabatic lapse rate ($\Gamma = 0.0098$ K/m). The temperature profiles were derived from measurements between the minimum aircraft height of 150 m and 300 m (agl). The profile was considered neutral if dT/dz was within 20% of Γ. Because the RASS profiles demonstrated very different lapse rates near the surface compared to further aloft, these data were separated into near-surface (<100m) and higher (>100m). The layered approach of Eq. 7 is based on the assumption of neutral or stable conditions. Since there is a relatively low frequency of unstable conditions in all cases (4% to 13%), any error caused by use of the method with $s < 0$ is likely small.

The profile measurements used for the layered method give a much different indication of stability class, with predominantly stable conditions between for 53% and 89% of the time. The RASS measurement profiles demonstrate a higher frequency of stable conditions near the surface (based on comparison to the lapse rate). For the RASS measurements, there is a significant difference between stability classifications based on Obukhov length compared to stability classifications based on the temperature lapse rate, suggesting that these two methods are not directly comparable.

Atmos. Chem. Phys. Discuss., https://doi.org/10.5194/acp-2017-1093
Manuscript under review for journal Atmos. Chem. Phys.
Discussion started: 20 December 2017

Based on previous studies summarized in VDI (1985), the authors suggested a reduction of the Briggs parameterization by 30% in neutral conditions. Although the atmospheric stability is predominantly classified as neutral in our analysis, we are seeing an underestimation by the Briggs parameterization, in contrast to the previous studies. Hence this discrepancy does not appear to be due to difference in stability regimes in the different studies.

4.2 Sensitivity to Input Variables

As a simple test of the sensitivity of the Briggs algorithm to uncertainties in input variables, average plume rise was recalculated with modified input variables. The average plume rise is calculated for the box and screen flight times for the 8 stacks used in the analysis. Input variables were then modified by an arbitrary fraction to determine the resulting change in average plume rise relative to the average plume rise calculated with unmodified input variables. As a conservative estimate of measurement uncertainty, air temperatures (at the surface and stack height) were varied by ±5% (approximately 15 K) and wind speeds were varied by ±20%. The values of H, u_*, and L, which are calculated using empirical formulae and least-squares fits (Eqns. 9-13) are varied by ±50%. Stack height and volume flow rate (h_s, V) are varied by ±20%, while effluent temperature (T_s) is varied by ±10%. Average percentage changes in the plume rise for each modification for each measurement platform are listed in Table 5. These values are not meant to accurately estimate uncertainty in the measurements, but are used only to demonstrate the change in plume rise relative to a substantial change in each input variable.

Table 5. Percent change in average plume height ($\Delta h(X \pm 5\%)/\Delta h(X)$), where X is the modified parameter (i.e. T_a, U, etc.). For example, ±5% for air temperature recalculates plume rise (Δh) with $0.95T_a$ (low) or $1.05T_a$ (high). The average is for the 46 flight hours (box and screen flight times) and 8 stacks used in the analysis. All values are given as %.

Variable	Units	Mod.	AMS03		AMS05		RASS	
		[%]	Low	High	Low	High	Low	High
T_a	K	±5	3.6	-4.1	3.7	-4.2	3.0	-5.2
U	m/s	±20	11.2	-8.4	11.3	-8.2	7.4	-6.3
$T_{surface}$	K	±5	0.0	0.0	-0.2	0.0	-1.6	0.0
H	m	±50	-20.0	8.6	-19.3	8.0	-30.9	18.1
u_*	m/s	±50	9.0	-15.4	3.5	-15.6	26.3	-21.6
L	m	±50	11.5	-6.9	16.6	-8.9	-4.6	7.9
h_s	M	±20	-4.3	6.5	-3.3	12.2	-1.4	3.3
T_s	K	±10	-9.9	6.3	-9.7	6.2	-9.3	5.1
V	m/s	±20	-8.2	7.1	-8.2	7.4	-7.3	6.3

The calculated plume rise is least sensitive to surface temperature ($T_{surface}$) and is most sensitive to boundary-layer height (H) and friction velocity (u_*). Reducing H by 50% could lead

Atmos. Chem. Phys. Discuss., https://doi.org/10.5194/acp-2017-1093
Manuscript under review for journal Atmos. Chem. Phys.
Discussion started: 20 December 2017

to a reduction in plume rise of 30%, while a 50% reduction in u_* can results in an increase in plume rise of more than 26%. This suggests that there may be significant uncertainty in the calculated plume rise due to the inherent uncertainty in these variables which are derived from parameterization. The table identifies the variables with the largest impact on the parameterization results, hence which variables require the greatest accuracy when obtained from a meteorological model forecast. These results also help explain the low correlation coefficients of the observation-driven plume rise height comparisons (Table 3), as uncertainty in the estimation of these derived quantities will lead to uncertainty in individual plume rise estimations.

4.3 Horizontal Distance to Plume Rise

If the stacks are physically close enough to the interception of the plume with the box walls or screens it may be the case that the plumes have not travelled a sufficient distance to reach the maximum plume rise that is parameterized by the Briggs algorithms. Briggs (1984) also developed parameterizations of downwind distance to maximum plume rise. A plume in stable conditions will reach its final rise (Briggs, 1984) at

$$x_e = 4.7\left(\frac{U}{\sqrt{s}}\right). \tag{14}$$

A plume in neutral conditions will reach its final rise (Briggs, 1975) at

$$x_e = \begin{cases} 49F_b^{5/8} & \text{for } F_b < 55\ \mathrm{m^4 s^{-3}} \\ 119F_b^{2/5} & \text{for } F_b > 55\ \mathrm{m^4 s^{-3}} \end{cases} \tag{15}$$

In unstable conditions, the plume fumigates and is evenly distributed in concentration between the surface and a height of $1.5\Delta h$, based on the assumption that the half-width of the plume is $0.5\Delta h$. Although no parameterization has been developed for the distance required to reach maximum plume rise in unstable conditions, Briggs (1984) provides a parameterization of the average horizontal distance to fumigation (contact of the plume with the surface) as

$$x_f = \frac{U}{w}(h_s + 0.5\Delta h), \tag{16}$$

where the average downdraft speed is $w = 0.8u_*$, following Briggs (1984).

Using the AMS03 input data as an example, none of the 87 matched plumes have distance from stack to measurement location (x_d) less than the horizontal distance to reach maximum plume rise ($x_d < x_e$) in neutral or stable cases, or less than the distance to fumigation ($x_d < x_f$) in unstable cases. As discussed above, the analysis is limited to plume sources that are within 50 km of the box walls or screens. The distances between stacks and box walls (following the forward trajectories) range from 4 to 16 km, while the distances between stacks and screens ranges from 3 km to more than 150 km. There are 33 screens with matching plume observations within 40 km of the stack sources and 38 screens with matching plume observations more than 60 km of the stack sources (there are none in the 40 – 60 km range). Tests demonstrate (not shown) that including the 38 screen plume observations beyond 60 km from the sources in the analysis results in lower correlations and poorer performance of the Briggs parameterizations, as expected.

Atmos. Chem. Phys. Discuss., https://doi.org/10.5194/acp-2017-1093
Manuscript under review for journal Atmos. Chem. Phys.
Discussion started: 20 December 2017

Atmospheric Chemistry and Physics Discussions

The distance to reach maximum plume rise or fumigation based on Eqns. 14-16 is not more than 2 km for all of the 87 plumes in this analysis. Hence it can be assumed that all measurement locations were far enough downwind that the plumes should have reached their highest trajectory. For model resolutions of greater than 2 km (c.f. Akingunola et al, 2017), the plumes will all have reached their equilibrium height within one grid-square distance of emission. Had the measurements been too close to the stacks, some overestimation may have occurred due to the measured plumes not reaching their maximum height. However, that does not appear to be the case here.

4.4 Modifications to the Plume Equations

4.4.1 Minimum Criteria

As discussed in Section 2.1, the minimum criteria of Eqns. 4 and 5, which are used in the GEM-MACH model are not used in other plume rise models, such as SMOKE. To investigate the difference between these two approaches, the plume rise is recalculated using only the right term within the minimum functions of Eqns. 4 and 5. The resulting statistics are listed in Table 3.

This results in slightly higher slopes of the least-squares fit and higher average ratios of predicted to observed plume rise. The average ratio is 13% higher using the AMS03 data, and 3 or 4% higher using the AMS05 or RASS data. The percentage of predicted plume rise values which are within a factor of 2 of the observed values is increased by 3% for the RASS data, but decreases 2% and 1% for the AMS03 and AMS05 data owing to an increase in the number of values which are over-predicted by more than a factor of 2. Hence, there is still a significant amount (37 to 41%) of plume heights which are under-predicted by more than a factor of 2, even without the use of the minimum criteria.

4.4.2 Effluent Momentum

To compare the effects of initial effluent momentum on plume rise, we use the Briggs parameterizations for momentum-dominated plumes as given in de Visscher (2013). These are given for stable and neutral conditions respectively as

$$\Delta h_m = 1.5\left(\frac{F_m}{Us^{1/2}}\right)^{1/3}, \quad \Delta h_m = 3\left(\frac{F_m}{U^2}\right)^{1/2}, \tag{17}$$

where the momentum flux is

$$F_m = \left(\frac{T_a}{T_s}\right)\frac{d_s^2 w_s^2}{4}. \tag{18}$$

For unstable conditions, the parameterization of Eq. 8 is used.

Plumes are typically classified as either momentum driven or buoyancy driven, and the maximum of Δh and Δh_m is used to estimate plume rise (e.g. Briggs, 1984; VDI, 1985). Here we add Δh and Δh_m together to give an upper limit of plume rise due to both momentum and buoyancy. Since removal of the minimum criteria (discussed above) improved the results slightly, this is combined with addition of momentum to determine the added effect of both improvements. The summary statistics are compared to those due to buoyancy alone in Table 3. Results are generally improved, with a 6 to 9% increase in the average ratio of predicted to

observed plume rise. However, more than a third (34 to 40%) of the predicted plume rise values are still underestimated by more than a factor of 2, even though the addition of buoyancy and momentum effects is considered to be an upper limit.

5. Conclusions

These results demonstrate a significant underestimation of plume rise using the Briggs plume rise parameterizations. The ratio of average modelled plume rise to average measured plume rise ($\sum h_{B,i}/\sum h_{M,i}$) varies from 0.51 to 0.87, depending on the method (Briggs parameterization or layered method) and platform (aircraft, RASS, or tower) used to measure input variables. This range of ratios suggests an average underestimation between 13 and 49%. Results are improved slightly by including plume rise due to the initial momentum at the stack exhaust and the removal of the minimum criteria from the plume rise equations. Including these modifications suggests an average underestimation between 4 and 21%.

These results are in direct contrast to the many studies summarized in VDI (1985), which consistently suggest that plume rise is overestimated by the Briggs equations. Only the more recent study of Webster and Thomas (2002) might imply an underestimation of plume rise, owing to an overestimation of surface concentration measurements using a plume rise model. The authors of the VDI report suggest that the Briggs parameterization should be reduced by a factor of 30% in neutral conditions in order to better match observations. In contrast to this suggestion, our results would be improved significantly by increasing the Briggs parameterization by a factor of 30%.

For both the Briggs parameterization and layered method and for all the measurement platforms used in this study, the correlation of parameterized plume rise to measured plume rise is low ($r^2 \leq 0.2$) and the slopes of the least-squares fits are less than or near 0.5. Moses and Carson (1969) stated that “no plume rise equation can be expected to accurately predict short term plume rise” and that their parameterizations were “to be used for general design considerations.” This statement appears to remain true nearly 50 years later and the wide use of these same equations in air quality models indicates that little improvement has been made.

The aircraft-based measurements used for this study provide only a “snapshot” of plume rise and atmospheric conditions as measurements are made on a timescale of a few hours in the morning or afternoon over the course of a few weeks in summer. However, this consistent underestimation of plume height for these observations suggest that further investigation is warranted. Given the advancements in atmospheric measurement technology in recent decades (e.g. automated lidar, RASS, image analysis), there is an opportunity to make long-term measurements of plume rise and atmospheric conditions in an effort to improve predictability. Although the Briggs algorithms have been in use for nearly 4 decades, are used in many air-quality models (e.g. GEM-MACH, AEROPOL, SCREEN3, CALGRID, RADM, SMOKE, and SMOKE-EU), and are widely referenced in air quality and dispersion texts (Beychok and Milton, 2005; Arya, 1998), the verification of these algorithms relies on decades old measurement techniques. More in-situ measurements of plume height are clearly needed to attempt to quantify the uncertainties in these parameterizations and to suggest improvements to the algorithm.

Acknowledgements

The authors wish to thank the Wood Buffalo Environmental Association (WBEA) for the use of the Lower Camp Met Tower (AMS03) and Mannix Tower (AMS05) data. The Continuing Emission Monitoring System (CEMS) data were provided by Marilyn Albert, Ewa Przybylo-Komar, Katelyn Mackay, and Tara-Lynn Carmody of Data Management and Stewardship, Corporate Services Division, Alberta Environment and Parks.

References

A. Akingunola, P.A. Makar, M.D. Moran, J, Zhang, Q. Zheng, S.-M. Li (2017), Simulations of Oil Sands Emissions, Transformation and Fate using the GEM-MACH Model: The impacts of plume rise and particle size resolution. *Atmos. Chem. Phys.* This issue.

S.P. Arya (1998) Air Pollution Meteorology and Dispersion (1st ed.). Oxford University Press.

M.R. Beychok (2005). Fundamentals Of Stack Gas Dispersion (4th ed.). author-published

J. Bieser, A. Aulinger, V. Matthias, M. Quante, P. Builtjes (2011a) SMOKE for Europe – adaptation, modification and evaluation of a comprehensive emission model for Europe. *Geoscientific Model Development*, 4, 47-68. doi:10.5194/gmd-4-47-2011

J. Bieser, A. Aulinger, V. Matthias, M. Quante, H.A.C. Denier van der Gon (2011b) Vertical emission profiles for Europe based on plume rise calculations, *Environ. Pollut.*, 159, 2935-2946. doi:10.1016/j.envpol.2011.04.030

G.A. Briggs (1969) Plume rise. Report for U.S. Atomic Energy Commission, Division of Technical Information.

G.A. Briggs (1975) Plume rise predictions, Lectures on air Pollution and environmental impact analyses. In: Workshop Proceedings, Sept. 29-Oct. 3, pp. 59-111. Boston, MA, USA.

G.A. Briggs (1984) Plume rise and buoyancy effects, atmospheric sciences and power production. In: Randerson, D. (Ed.), DOE/TIC-27601 (DE84005177), TN. Technical Information Center, U.S. Dept. of Energy, Oak Ridge, USA, p. 850.

G,A, Briggs (1985) Analytical parameterizations of diffusion: the convective boundary layer, *J. Clim. Appl. Meteor.*, 24, 1167–1186.

D.W. Byun, F.S. Binowski (1991) Sensitivity of RADM to point source emissions processing. In: Paper 5.4 presented at the 7th Joint conference on Applications of Air Pollution Meteorology with the Air and Waste Management Association, Jan. 14-18, 1991, New Orleans, LA. American Meteorological Soc, Boston, MA, USA, pp. 70e73.

D.W. Byun, J.K.S. Ching (1999) Science algorithms of the EPA Models-3 community multiscale air quality (CMAQ) modeling system, US EPA, Office of Research and development, EPA/600/R-99/030.

J.E. Carson and H. Moores (1969) The Validity of Several Plume Rise Formulas, J. Air Pollut. Control. 19:11, 862-866, doi:10.1080/00022470.1969.10469350

CEMA (2012) Lower Athabasca Region Source and Emission Inventory, Prepared for Cumulative Environmental Management Association, Ft McMurray, AB, April 16, 2012, ENVIRON CA12-00394A, Stantec 123510559 (T210).

CEMS (1998) Continuous Emission Monitoring System (CEMS) Code, Alberta Environmental Protection, Pub. No. Ref. 107, ISBN: 0-7732-5038-7.

CMAS Website, https://www.cmascenter.org/smoke/, last accessed Nov., 2017.

J. Côté, S. Gravel, A. Méthot, A. Patoine, M. Roch, and A. Staniforth (1998) The Operational CMC–MRB Global Environmental Multiscale (GEM) Model. Part I: Design Considerations and Formulation. *Mon. Wea. Rev.*, 126, 1373–1395, doi: 10.1175/1520-0493(1998)126<1373:TOCMGE>2.0.CO;2.

J. Cuxart, J. Cunillera, M.A Jiménez, D. Martínez, F. Molinos, J.L. Palau (2011) Study of Mesobeta Basin Flows by Remote Sensing, *Bound.-Lay. Meteor.* 143 (1), 143-158. doi:10.1007/s10546-011-9655-8

ECCC & AEP (2016) Environment and Climate Change Canada & Alberta Environment and Parks: Joint Oil Sands Monitoring Program Emissions Inventory Compilation Report, http://aep.alberta.ca/air/reports-data/documents/JOSM-EmissionsInventoryReport-Jun2016.pdf, 146 pp, last accessed Nov., 2017.

C. Emery, K. Jung, G. Yarwood (2010) Implementation of an Alternative Plume Rise Methodology in CAMx. Final Report, Work Order No. 582-7-84005-FY10-20.

J.R. Garratt (1994) The atmospheric boundary layer (1st ed.). Cambridge University Press.

J. Gielbel (1979) Messungen der Abgasfahnenüberhöhung eines Steinkohlekraftwerkes mit Hilfe von LIDAR (Plume Rise measuremetns of a pit coal power plant by means of LIDAR). (German) Schriftenreihe der Landesanstalt fur Immissionsschutz des Landes NRW, Heft 47, S. 42/59.

M. Gordon, S.-M. Li, R. Staebler, A. Darlington, K. Hayden, J. O'Brien, M. Wolde (2015) Determining air pollutant emission rates based on mass balance using airborne measurement data over the Alberta oil sands operations, *Atmos. Meas. Tech.*, 8, 3745-3765, doi:10.5194/amt-8-3745-2015.

N.S. Holmes, L. Morawska (2006) A review of dispersion modelling and its application to the dispersion of particles: An overview of different dispersion models available. *Atmos. Env.* 40 (30), 5902-5928. doi: 10.1016/j.atmosenv.2006.06.003.

M.R. Houyoux (1998) Technical Report: Plume Rise Algorithm Summary for the Sparse Matrix Operator Modeling System (SMOKE). North Carolina Department of Environment and Natural Resources, UNC, Chapel Hill, North Carolina, ENV-98TR004eTR0v1.0.

U. Im, R. Bianconi, E. Solazzo, I. Kioutsioukisa, A. Badiac, A. Balzarinid, R. Baróe, R. Bellasio, D. Brunner, C. Chemel, G. Curcih, H. Denier van der Gon, J. Flemming, R. Forkel, L. Giordano, P. Jiménez-Guerrero, M. Hirtl, A. Hodzic, L. Honzak, O. Jorbac, C. Knotem, P.A.Makar, A. Manders-Groot, L. Neal, J.L. Pérez, G. Pirovano, G. Pouliot, R.S. Jose, N.

Savage, W. Schroder, R.S. Sokhi, D. Syrakov, A. Torian, P. Tuccella, K. Wang, J. Werhahnk, R. Wolke, R. Zabkarn, Y. Zhang, J. Zhang, C. Hogrefe, S. Galmarinia (2015) Evaluation of operational online-coupled regional air quality models over Europe and North America in the context of AQMEII phase 2. Part II: Particulate matter, *Atm. Env.*, 115, 421-441. doi:10.1016/j.atmosenv.2014.08.072

J.C. Kaimal and J.J. Finnigan (1994) Atmospheric Boundary Layer Flows: Their Structure and Measurement (1st ed.), Oxford University Press.

S.-M. Li, A. Leithead, S.G. Moussa, J. Liggio, M.D. Moran, D. Wang, K. Hayden, A. Darlington, M. Gordon, R. Staebler, P.A. Makar, C. Stroud, R. McLaren, P.S.K. Liu, J. O'Brien, R. Mittermeier, J. Zhang, G. Marson, S. Cober, M. Wolde, J. Wentzell (2017) Differences between Measured and Reported Volatile Organic Compound Emissions from Oil Sands Facilities in Alberta, Canada. *Proc. Natl. Acad. Sci.*, 114, 19, E3756-E3765. doi: 10.1073/pnas.1617862114

J. Liggio, S.-M. Li, K. Hayden, Y.M. Taha, C. Stroud, A. Darlington, B.D. Drollette, M. Gordon, P. Lee, P. Liu, A. Leithead, S.G. Moussa, D. Wang, J. O'Brien, R.L. Mittermeier, J. Brook, G. Lu, R. Staebler, Y. Han, T.T. Tokarek, H.D. Osthoff, P.A. Makar, J. Zhang, D. Plata, D.R. Gentner (2016) Oil sands operations are a major source of secondary organic aerosols, *Nature*, 534, 91–94. doi:10.1038/nature17646.

P.A. Makar., W. Gong, J. Milbrandt, C. Hogrefe, Y. Zhang, G. Curci, R. Zabkar, U. Im, A. Balzarini, R. Baro, R. Bianconi, P. Cheung, R. Forkel, S. Gravel, H. Hirtl, L. Honzak, A. Hou, P. Jimenz-Guerrero, M. Langer, M.D. Moran, B. Pabla, J.L. Perez, G. Pirovano, R. San Jose, P. Tuccella, J. Werhahn, J. Zhang, S. Galmarini (2015) Feedbacks between air pollution and weather, part 1: Effects on weather. *Atm. Env.*, 115, 442-469. doi:/10.1016/j.atmosenv.2014.12.003

P.A. Makar., W. Gong, C. Hogrefe, Y. Zhang, G. Curci, R. Zabkar, J. Milbrandt, U.,Im, A. Balzarini, R. Baro, R. Bianconi, P. Cheung, R. Forkel, S. Gravel, H. Hirtl, L. Honzak, A. Hou, P. Jimenz-Guerrero, M. Langer, M.D. Moran, B. Pabla, J.L Perez, G. Pirovano, R. San Jose, P. Tuccella, J. Werhahn, J. Zhang, S. Galmarini, (2015) Feedbacks between air pollution and weather, part 2: Effects on chemistry. *Atm. Env.*, 115, 499-526. doi:10.1016/j.atmosenv.2014.10.021

P.A. Makar, R.M. Staebler, A. Akingunola, J. Zhang, C. McLinden, S.K. Kharol, B. Pabla, P. Cheung, Q. Zheng (2017) The effects of forest canopy shading and turbulence on boundary layer ozone, *Nature Communications*, 8. doi:10.1038/ncomms15243

NPRI website, http://ec.gc.ca/inrp-npri, last accessed Nov., 2017.

L. Mahrt (1981) Modelling the depth of the stable boundary-layer. *Bound.-Lay. Meteor.*, 21, 3–19. doi:10.1007/BF00119363.

S. Ménard, S. Gravel, M.D. Moran, H. Landry, A. Kallaur, R. Pavlovic, P.A. Makar, C. Stroud, W. Gong, J. Chen, D. Anselmo, S. Cousineau (2014) Current and Future Developments in Numerical Air Quality Forecasting in Canada. In: Steyn D., Mathur R. (eds) Air Pollution

Modeling and its Application XXIII. Springer Proceedings in Complexity. Springer, Cham, doi:10.1007/978-3-319-04379-1_104

T. Pregger, R. Friedrich (2009) Effective pollutant emission heights for atmospheric transport modelling based on real-world information. *Environ. Pollut.* 157 (2), 552-560. doi:10.1016/j.envpol.2008.09.027.

G. Sharf, M. Peleg, M. Livnat, M. Luria (1993) Plume rise measurements from large point sources in Israel, *Atomos. Environ.*, 27A, 1657 – 1663. doi.org/10.1016/0960-1686(93)90228-Q

VDI (1985) Ausbreitung von Luftverunreinigungen in der Atmosphäre; Berechnung der Abgasfahnen-überhöhung. (Dispersion of air pollutants in the atmosphere; determination of plume rise) 1985-06 (German/English), Kommission Reinhaltung der Luft (KRdL) im VDI und DIN – Normenausschuss, Available from: http://www.vdi.de.

A. de Visscher (2013) Air Dispersion Modeling: Foundations and Applications. Wiley. pp 664.

H.N. Webster, D.J. Thomson (2002) Validation of a Lagrangian model plume rise scheme using the Kincaid data set. *Atmos. Environ.*, 36, 5031–5042

J. Zhang, M.D. Moran, Q. Zheng, P.A. Makar, P. Baratzadeh, G. Marson, P. Liu, and S.M. Li. Emissions preparation and analysis for air quality modelling for the JOSM project over the Athabasca oil sands region of Alberta, Canada, *Atmos. Chem. Phys.* This issue.